

Semi-automatic segmentation and surface reconstruction of computed tomography images by using roto-scoping and warping techniques

S.K. Park, B.K. Kim, D.S. Shin

Department of Emergency Medical Technology, Gachon University of College of Health Science, Incheon, South Korea

[Received: 11 March 2019; Accepted: 9 April 2019]

Background: Quick and large-scale segmentation along with three-dimensional (3D) reconstruction is necessary to make precise 3D musculoskeletal models for surface anatomy education, palpation training, medical communication, morphology research, and virtual surgery simulation. However, automatic segmentation of the skin and muscles remain undeveloped.

Materials and methods: Therefore, in this study, we developed workflows for semi-automatic segmentation and surface reconstruction, using roto-scoping and warping techniques.

Results: The techniques were applied to multi detector computed tomography images, which were optimised to quickly generate surface models of the skin and the anatomical structures underlying the fat tissue.

Conclusions: The workflows developed in this study are expected to enable researchers to create segmented images and optimised surface models from any set of serially sectioned images quickly and conveniently. Moreover, these optimised surface models can easily be modified for further application or educational use. (Folia Morphol 2020; 79, 1: 156–161)

Key words: cross-sectional anatomy, segmentation, surface reconstruction, three-dimensional imaging, landmark, surface anatomy, roto-scoping

INTRODUCTION

Segmentation and surface reconstruction of anatomical structures from medical images form an essential step for designing a surgical plan or conducting a morphological research. Several methods and pieces of software have been developed for segmentation and surface reconstruction [5, 8, 9, 17, 31]. However, automatic segmentation of the skin and the muscles remain undeveloped owing to the ambiguous boundaries between them and the neighbouring structures.

Superficial anatomy is based on projections of the major organs of human body, with the help of surface

landmarks. It deals with anatomical features that can be observed by sight, without dissection. In addition, it includes the theories and systems pertaining to the proportions of the human body and location of surface landmarks that may relate to the deeper anatomical structures [1, 2, 4, 7, 10, 15, 16, 18–20, 29, 30].

In this study, we developed workflows for semi-automatic segmentation and surface reconstruction with the help of roto-scoping and warping techniques, derived from the field of graphic design and animation. By using the workflows developed in this study, optimised and small-sized surface models with respect to superficial anatomy can be made. These surface models

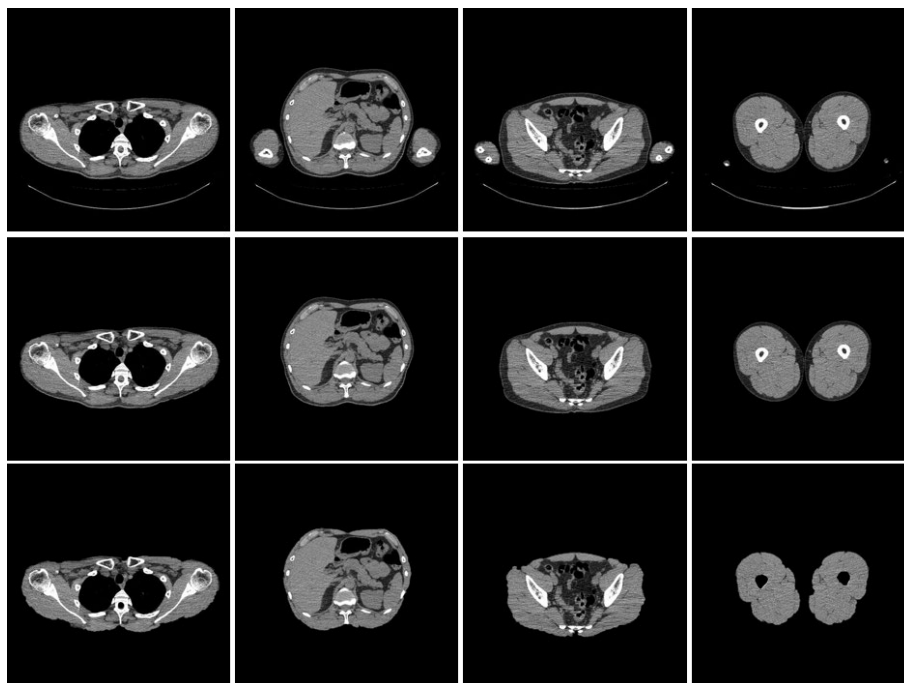


Figure 1. Multi-detector computed tomography (MDCT) images: Original images (top line), segmented images of skin (middle line), and segmented images of structures underlying the fat tissue (bottom line).

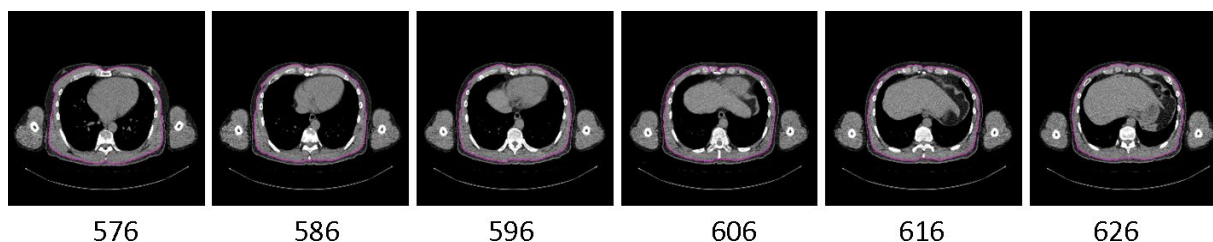


Figure 2. Outline of structures underlying the fat tissue is semi-automatically drawn in 576th and 626th images, wherein the outline of the intervening 48 images are drawn automatically using the roto-scoping technique.

can be three-dimensionally (3D) displayed in a portable document format (PDF) file. Additionally, the surface models and stereoscopic structures can be related with the displayed landmarks in real time [24–28].

The workflows developed in this study are expected to enable researchers to create segmented images and optimised surface models from any set of serially sectioned images quickly and conveniently. Moreover, they can be translated into different formats, and easily modified for further application or educational use owing to their small file size and optimized surface structure.

MATERIALS AND METHODS

Semi-automatic segmentation

Multi-detector computed tomography (MDCT) scans (Siemens, SOMATOM definition AS+ 128; reso-

lution: 512×512 , interval: 1 mm) were obtained from a 41-year-old male (stature: 1.75 m, weight: 71 kg; Fig. 1). The acquired MDCT images (1,332) were opened using After Effects version CC 2015 (Adobe, San Jose, California, United States). Subsequently, the skin and the anatomical structures underlying the fat tissue were outlined.

Firstly, outline of skin was drawn semi-automatically only in one of the images using 'Roto Brush Tool', which was followed by automatic outlining in the next 30 to 50 images (Fig. 2).

Secondly, incorrectly generated outlines owing to the unclear skin boundaries were refined semi-automatically. They were also partially refined using the 'Roto Brush Tool'. In case of the anatomical structures underlying the fat tissue, boundary between the fat, bones, and muscles were not clear than that of the

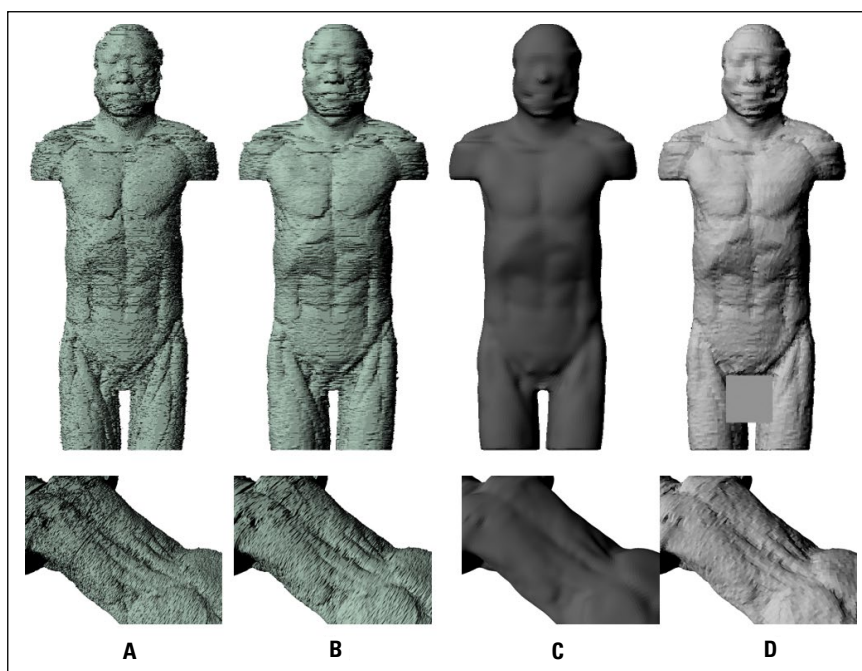


Figure 3. Surface models of the anatomical structures underlying the fat tissue, front view (top line) and back view (bottom line). Highest-quality surface model (A), low-quality surface model (B), reduced surface model (C), and warped surface model (D).

skin. Therefore, the outlines in 10 to 20 images were automatically generated after manual intervention. During automatic outline generation, the unnecessary outline of inner structure, such as that of intestine, was also drawn. However, the inner outline can be removed easily in the next step of 3D reconstruction. Therefore they were ignored in this step. Consequently, 2 sets of segmented images of the skin and the structures underlying the fat tissue were constructed.

3D reconstruction

All the 1,332 segmented images of the skin and the anatomical structures underlying the fat tissue were opened using Mimics version 16.1, which has several options for surface reconstruction (Materialise, Leuven, Belgium) [24–28]. The segmented images were surface-reconstructed (Fig. 3A, 3B) using both the highest-quality and low-quality options of the Mimics. The highest-quality surface models have a large file size, which is difficult to display. Therefore, low-quality surface models were wrapped using the highest-quality model in the next step. As a result, two sets (highest quality and low quality) of images for the skin and the structures underlying the fat tissue were obtained. During surface reconstruction procedure, the unnecessary inner structures that were outlined in the segmentation procedure were easily removed by means of clicking. Hence, two surface models were

saved as stereolithography (STL) files, which were subsequently accessed using Maya software.

Optimisation and morphing

The surface models were subsequently optimised and labelled using Maya version 2018 (Autodesk, Inc., San Rafael, California, USA) and ZBrush 4 (Pixologic Inc, Los Angeles, California, USA) [26]. The imported highest-quality surface models had a more realistic shape than the low-quality surface models; however, they consisted of triangular polygonal structures with large numbers of polygons. Triangular polygonal structures are difficult to refine and label. Moreover, large files are difficult to display on multiple devices. Therefore, we used warping technique to make optimised surface models [26].

Firstly, triangular structure of the low-quality surface model was quadrangulated automatically by using 'zRemesher' function of the ZBrush software.

Secondly, the number of quadrangulated surfaces was decreased as much as possible without compromising the original shape of the anatomical structures, using the 'zRemesher' function of the ZBrush software (Fig. 3C) [26]. During this procedure, the detailed shape of the anatomical features was simplified, which was recovered in the next step.

Thirdly, the simplified regions were recovered by '3D morphing' technique using 'ShrinkWarp' function

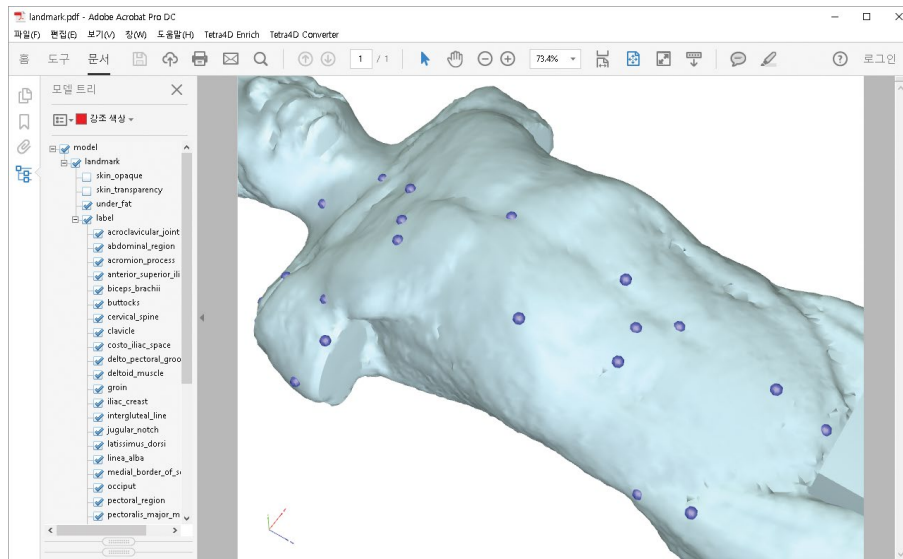


Figure 4. The name of the surface model is displayed in the left window (model tree), while the surface model is exhibited in the right window of the PDF file.

of the Maya software. The low-quality surface model was overlapped with the highest-quality surface model to recover the simplified regions (Fig. 3D) [26]. As a result, the shape obtained by the low-quality surface model changed to that of the highest-quality models. This process resulted in creation of the optimised surface models.

Labelling and converting into a PDF file

The body landmarks in the optimised surface models were annotated by anatomists. 3D spheres were made, and moved to the region of body landmarks, and named as the landmarks [27, 28]. As a result, 36 3D spheres corresponding to the body landmarks were made on the surface model that depicted the anatomical structures underlying the fat tissue (Table 1). All the 3D spheres and the surface models were saved as STL files, which were subsequently sent to the next software package.

Surface models were arranged using Deep Exploration Standard (Right Hemisphere, San Ramon, California, USA). The arranged STL files were saved as WRL (file extension for a virtual reality modelling language [VRML] file format) files. The surface models saved in the WRL format were transported to a PDF file. We used the previously formulated and detailed transfer methods [21, 27, 30].

Previously, the procedure was conducted using the 3D Reviewer, a software that accompanies the Acrobat 9.0 Pro Extended (Adobe Systems, San Jose, CA) [21, 23, 27]. However, the use of this software is now dis-

Table 1. The 39 structures of surface models and body landmarks was made

Surface models (3)

skin transparency, skin opaque, under fat

Body landmarks (36)

abdominal region, acroclavicular joint, acromion process, anterior-superior iliac spine, biceps brachii, buttocks, cervical spine, clavicle, costo-iliac space, delto-pectoral groove, deltoid muscle, groin, iliac crest, intergluteal line, jugular notch, latissimus dorsi, linea alba, medial border of scapula, occiput, pectoral region, pectoralis major muscle, pubic region, ribs, sacral dimple, scapula, spinal muscles, spine of scapula, spinous process, sternum, subgluteal line, thoracic spine, trapezius, triceps brachii, umbilicus, xiphoid notch, sternocleidomastoid muscle

continued. Thus, we used another software, Tetra4D Converter (Tech Soft 3D, Inc., Ashby Avenue Berkeley, CA), to transfer the surface models to a PDF file. The name of the surface model was displayed in the left window (model tree), while the surface model was exhibited in the right window of the PDF file (Fig. 4).

RESULTS

The use of After Effects, Mimics, Maya, ZBrush, and Deep Exploration Standard enabled generation of surface models for superficial anatomy of human body using MDCT images.

The surface models can be 3D displayed in a PDF file. They can be translated into different formats and easily modified according to the purpose owing to their small size and optimised surface structure. When a user clicks a landmark point, its anatomic name is highlighted in the left tree window. Reverse

highlighting is also possible, wherein clicking on text in the left tree window displays the corresponding landmarks. Additionally, the surface models and stereoscopic structures related with the landmarks can be displayed in real time.

Because of the small file size, the surface models can be used in 3D applications on mobile devices. As an example of an on-line use, we tested the real-time display performance. Unlike surface models in the PDF file, the on-line uploaded surface models can be displayed on smart phones and internet browsers [26].

The PDF file (size: 1.3 MB) is available in the form of a supplement file of this paper (**Suppl. Fig. 1** — see **journal website**). PDF file with surface models and landmarks). Moreover, the source files, including the original MDCT images, segmented images, surface models, and optimised surface models are available through a direct email request to the corresponding author. Our data sharing policy allows free downloading and does not require registration.

DISCUSSION

Semi-automatic outlining methods have been previously discussed using visible human dataset [11, 12, 14, 22–24]. In this study, we suggested more advanced and quicker methods based on techniques of graphic design and animation. We used several software packages, namely, After Effects, Mimics, ZBrush, Maya, Deep Exploration, and Tetra4D.

Every software package has its own set of useful functions; however, no single software can contain all the necessary functions. Thus, we used multiple pieces of software in this study. In the segmentation step, some inner structures were automatically outlined, and some regions were incorrectly selected between the skin and the outside surface. These misselected structures, especially the unintended regions, such as the lungs, were easily deleted after surface reconstruction, using the surface-reconstruction software. Maya software aids in optimisation of the images; however, the quality is not good, and the process is semi-automatic. Conversely, ZBrush software has a strong optimisation function. Thus, we only used this function of the ZBrush. Deep Exploration software was used as a bridge between Maya and Tetra4D. Both these pieces of software have an arrange function, but the function is hard to handle. Therefore, we used the software only for arrangement.

In this study, we developed innovative and quick methods for segmentation and surface reconstruction

of computed tomography (CT) images using new techniques of graphic design and animation.

Rotoscoping is an animation technique used in motion graphics. Designers use it to trace over movie footage, frame by frame, to separate a specific region. Shape of structures in the CT images also change smoothly like a movie. Therefore, we assumed that the image slices of body can be used as a movie sequence. Additionally, we assumed that the skin and the structures underlying the fat tissue can be the objects to be separated from the movie. Among the various rotoscoping pieces of software, After Effects has an automatic rotoscoping function. It automatically changes the shape of the subsequent images after drawing the shape of one image. Therefore, we used this function of the software for segmentation.

The rotoscoping technique was applied to the skin and anatomical structures underlying the fat tissue. Automatic segmentation of the fat tissue and the muscles in CT images is difficult. Many segmentation methods have been developed to segment skin, bone, heart, and air passage, as they have different Hounsfield units (HU) than the neighbouring structures. However, the HU of the muscles is almost same as that of the neighbouring structures, making their segmentation difficult [3, 5, 6, 8, 9, 13, 17, 31].

Warping is another 3D animation technique for character motion. We used this function to optimise the surface models. Detailed surface models obtained from CT, magnetic resonance imaging, or 3D scanning, have large file sizes that cannot be displayed or handled in real time. Therefore, the surface models were reduced, however, after reduction the detailed regions disappeared. Therefore, by using the warping function in Maya software, reduced surface model was warped to detailed surface model, and the disappeared regions were recovered with reduced surfaces.

The animation techniques used in this study can segment the target structures from the neighbouring structures with similar HUs, such as all the muscles, digestive system, and respiratory system. Moreover, these techniques are commonly used in the design field. Therefore, segmentation can be easily done even by a medical trainee or a student, in addition to a technician or a medical expert.

Quick and large-scale segmentation along with 3D reconstruction is necessary for designing a surgical plan or conducting a morphological research. The workflows developed in this study are expected to enable researchers to create segmented image and

optimised surface models from any set of serially sectioned images quickly and conveniently. Moreover, the optimised surface models can be easily modified for further application or educational use.

CONCLUSIONS

Generally, CT machines are limited in terms of scan length. In this study, we used the 128-channel MDCT scanner (Siemens, SOMATOM Definition AS+128). Maximum scan length of this machine is 1.7 m; however, the height of our volunteer (corresponding author) was 1.76 m. Therefore, the image was cut at the thigh. We intend to create landmarks for the whole body in our future studies, using another scanning machine with a suitable volunteer.

REFERENCES

1. Badshah M, Soames R, Ibrahim M, et al. Surface anatomy of major anatomical landmarks of the neck in an adult population: A CT Evaluation of Vertebral Level. *Clin Anat.* 2017; 30(6): 781–787, doi: [10.1002/ca.22907](https://doi.org/10.1002/ca.22907), indexed in Pubmed: [28514499](https://pubmed.ncbi.nlm.nih.gov/28514499/).
2. Badshah M, Soames R, Khan MJ, et al. Revisiting thoracic surface anatomy in an adult population: A computed tomography evaluation of vertebral level. *Clin Anat.* 2017; 30(2): 227–236, doi: [10.1002/ca.22817](https://doi.org/10.1002/ca.22817), indexed in Pubmed: [27935171](https://pubmed.ncbi.nlm.nih.gov/27935171/).
3. Dong X, Lei Y, Wang T, et al. Automatic multiorgan segmentation in thorax CT images using U-net-GAN. *Med Phys.* 2019; 46(5): 2157–2168, doi: [10.1002/mp.13458](https://doi.org/10.1002/mp.13458), indexed in Pubmed: [30810231](https://pubmed.ncbi.nlm.nih.gov/30810231/).
4. Fischer NJ, Morreau J, Sugunesegran R, et al. A reappraisal of pediatric thoracic surface anatomy. *Clin Anat.* 2017; 30(6): 788–794, doi: [10.1002/ca.22913](https://doi.org/10.1002/ca.22913), indexed in Pubmed: [28514496](https://pubmed.ncbi.nlm.nih.gov/28514496/).
5. Gargiulo P, Helgason T, Ramon C, et al. CT and MRI Assessment and Characterization Using Segmentation and 3D Modeling Techniques: Applications to Muscle, Bone and Brain. *Eur J Transl Myol.* 2014; 24(1): 3298, doi: [10.4081/ejtm.2014.3298](https://doi.org/10.4081/ejtm.2014.3298), indexed in Pubmed: [26913129](https://pubmed.ncbi.nlm.nih.gov/26913129/).
6. Hu P, Wu Fa, Peng J, et al. Automatic abdominal multi-organ segmentation using deep convolutional neural network and time-implicit level sets. *Int J Comput Assist Radiol Surg.* 2017; 12(3): 399–411, doi: [10.1007/s11548-016-1501-5](https://doi.org/10.1007/s11548-016-1501-5), indexed in Pubmed: [27885540](https://pubmed.ncbi.nlm.nih.gov/27885540/).
7. Jain N, Bhargava A, Pareek V, et al. Does seed size and surface anatomy play role in combating phytotoxicity of nanoparticles? *Ecotoxicology.* 2017; 26(2): 238–249, doi: [10.1007/s10646-017-1758-7](https://doi.org/10.1007/s10646-017-1758-7), indexed in Pubmed: [28083774](https://pubmed.ncbi.nlm.nih.gov/28083774/).
8. Kamiya N, Zhou X, Chen H, et al. Automated segmentation of rectus abdominis muscle using shape model in X-ray CT images. *Conf Proc IEEE Eng Med Biol Soc.* 2011; 2011: 7993–7996, doi: [10.1109/IEMBS.2011.6091971](https://doi.org/10.1109/IEMBS.2011.6091971), indexed in Pubmed: [22256195](https://pubmed.ncbi.nlm.nih.gov/22256195/).
9. Kamiya N, Zhou X, Chen H, et al. Automated segmentation of psoas major muscle in X-ray CT images by use of a shape model: preliminary study. *Radiol Phys Technol.* 2012; 5(1): 5–14, doi: [10.1007/s12194-011-0127-0](https://doi.org/10.1007/s12194-011-0127-0), indexed in Pubmed: [21755416](https://pubmed.ncbi.nlm.nih.gov/21755416/).
10. Kianmehr N, Hasanzadeh A, Naderi F, et al. A randomized blinded comparative study of clinical response to surface anatomy guided injection versus sonography guided injection of hyaluronic acid in patients with primary knee osteoarthritis. *Int J Rheum Dis.* 2018; 21(1): 134–139, doi: [10.1111/1756-185X.13123](https://doi.org/10.1111/1756-185X.13123), indexed in Pubmed: [28791808](https://pubmed.ncbi.nlm.nih.gov/28791808/).
11. Kim BC, Chung MS, Kim HJ, et al. Sectioned images and surface models of a cadaver for understanding the deep circumflex iliac artery flap. *J Craniofac Surg.* 2014; 25(2): 626–629, doi: [10.1097/SCS.0000000000000645](https://doi.org/10.1097/SCS.0000000000000645), indexed in Pubmed: [24621709](https://pubmed.ncbi.nlm.nih.gov/24621709/).
12. Kim BC, Chung MS, Park HS, et al. Accessible and informative sectioned images and surface models of the maxillofacial area for orthognathic surgery. *Folia Morphol.* 2015; 74(3): 346–351, doi: [10.5603/FM.2015.0052](https://doi.org/10.5603/FM.2015.0052), indexed in Pubmed: [26339816](https://pubmed.ncbi.nlm.nih.gov/26339816/).
13. Kohlberger T, Sofka M, Zhang J, et al. Automatic multi-organ segmentation using learning-based segmentation and level set optimization. *Med Image Comput Comput Assist Interv.* 2011; 14(Pt 3): 338–345, doi: [10.1007/978-3-642-23626-6_42](https://doi.org/10.1007/978-3-642-23626-6_42), indexed in Pubmed: [22003717](https://pubmed.ncbi.nlm.nih.gov/22003717/).
14. Kwon K, Shin DS, Shin BS, et al. Virtual endoscopic and laparoscopic exploration of stomach wall based on a cadaver's sectioned images. *J Korean Med Sci.* 2015; 30(5): 658–661, doi: [10.3346/jkms.2015.30.5.658](https://doi.org/10.3346/jkms.2015.30.5.658), indexed in Pubmed: [25931800](https://pubmed.ncbi.nlm.nih.gov/25931800/).
15. Morris VB, Corrigan D, Sealy U, et al. Anatomy from the outside in: a new on-line surface anatomy guide. *J Anat.* 2016; 228(1): 24–25, doi: [10.1111/joa.12412](https://doi.org/10.1111/joa.12412), indexed in Pubmed: [26565814](https://pubmed.ncbi.nlm.nih.gov/26565814/).
16. Nadesan T, Keough N, Suleman FE, et al. Appraisal of the surface anatomy of the Thorax in an adolescent population. *Clin Anat.* 2019; 32(6): 762–769, doi: [10.1002/ca.23351](https://doi.org/10.1002/ca.23351), indexed in Pubmed: [30758865](https://pubmed.ncbi.nlm.nih.gov/30758865/).
17. Popuri K, Cobzas D, Esfandiari N, et al. Body composition assessment in axial CT images using fem-based automatic segmentation of skeletal muscle. *IEEE Trans Med Imaging.* 2016; 35(2): 512–520, doi: [10.1109/TMI.2015.2479252](https://doi.org/10.1109/TMI.2015.2479252), indexed in Pubmed: [26415164](https://pubmed.ncbi.nlm.nih.gov/26415164/).
18. Quiles C, Constantino JA, Gañán Y, et al. Stereophotogrammetric surface anatomy of the anterior cruciate ligament's tibial footprint: Precise osseous structure and distances to arthroscopically-relevant landmarks. *Knee.* 2018; 25(4): 531–544, doi: [10.1016/j.knee.2018.03.016](https://doi.org/10.1016/j.knee.2018.03.016), indexed in Pubmed: [29705076](https://pubmed.ncbi.nlm.nih.gov/29705076/).
19. Shen XH, Su BY, Liu JJ, et al. A reappraisal of adult thoracic and abdominal surface anatomy via CT scan in Chinese population. *Clin Anat.* 2016; 29(2): 165–174, doi: [10.1002/ca.22556](https://doi.org/10.1002/ca.22556), indexed in Pubmed: [26032163](https://pubmed.ncbi.nlm.nih.gov/26032163/).
20. Shen XH, Xue HD, Chen Yu, et al. A reassessment of cervical surface anatomy via CT scan in an adult population. *Clin Anat.* 2017; 30(3): 330–335, doi: [10.1002/ca.22847](https://doi.org/10.1002/ca.22847), indexed in Pubmed: [28192864](https://pubmed.ncbi.nlm.nih.gov/28192864/).
21. Shin DS, Chung MS, Park JS, et al. Portable document format file showing the surface models of cadaver whole body. *J Korean Med Sci.* 2012; 27(8): 849–856, doi: [10.3346/jkms.2012.27.8.849](https://doi.org/10.3346/jkms.2012.27.8.849), indexed in Pubmed: [22876049](https://pubmed.ncbi.nlm.nih.gov/22876049/).
22. Shin DS, Jang HG, Hwang SB, et al. Two-dimensional sectioned images and three-dimensional surface models for learning the anatomy of the female pelvis. *Anat Sci Educ.* 2013; 6(5): 316–323, doi: [10.1002/ase.1342](https://doi.org/10.1002/ase.1342), indexed in Pubmed: [23463707](https://pubmed.ncbi.nlm.nih.gov/23463707/).
23. Shin DS, Jang HG, Park JS, et al. Accessible and informative sectioned images and surface models of a cadaver head. *J Craniofac Surg.* 2012; 23(4): 1176–1180, doi: [10.1097/SCS.0b013e31825657d8](https://doi.org/10.1097/SCS.0b013e31825657d8), indexed in Pubmed: [22801119](https://pubmed.ncbi.nlm.nih.gov/22801119/).
24. Shin DS, Kim HJ, Kim BC. Sectioned images and surface models of a cadaver for understanding the free vascularised anterior rib flap. *Folia Morphol.* 2017; 76(1): 117–122, doi: [10.5603/FM.a2016.0035](https://doi.org/10.5603/FM.a2016.0035), indexed in Pubmed: [27830889](https://pubmed.ncbi.nlm.nih.gov/27830889/).
25. Shin DS, Lee S, Park HS, et al. Segmentation and surface reconstruction of a cadaver heart on Mimics software. *Folia Morphol.* 2015; 74(3): 372–377, doi: [10.5603/FM.2015.0056](https://doi.org/10.5603/FM.2015.0056), indexed in Pubmed: [26339820](https://pubmed.ncbi.nlm.nih.gov/26339820/).
26. Shin DS, Park SK. Surface Reconstruction and Optimization of Cerebral Cortex for Application Use. *J Craniofac Surg.* 2016; 27(2): 489–492, doi: [10.1097/SCS.0000000000002352](https://doi.org/10.1097/SCS.0000000000002352), indexed in Pubmed: [26854785](https://pubmed.ncbi.nlm.nih.gov/26854785/).
27. Shin DS, Shim YJ, Kim BC. Sectioned images and 3D models of a cadaver head with reference to dermal filler injection. *Ann Anat.* 2018; 217: 34–39, doi: [10.1016/j.aanat.2018.02.001](https://doi.org/10.1016/j.aanat.2018.02.001), indexed in Pubmed: [29481857](https://pubmed.ncbi.nlm.nih.gov/29481857/).
28. Shin DS, Shim YJ, Kim BC. Sectioned images and surface models of a cadaver head with reference to botulinum neurotoxin injection. *Folia Morphol.* 2018; 77(3): 564–569, doi: [10.5603/FM.a2018.0005](https://doi.org/10.5603/FM.a2018.0005), indexed in Pubmed: [29345721](https://pubmed.ncbi.nlm.nih.gov/29345721/).
29. Stern J. Surface anatomy of the trunk based on CT data. *Clin Anat.* 2016; 29(2): 130, doi: [10.1002/ca.22511](https://doi.org/10.1002/ca.22511), indexed in Pubmed: [25691286](https://pubmed.ncbi.nlm.nih.gov/25691286/).
30. Uzun C, Atman ED, Ustuner E, et al. Surface anatomy and anatomical planes in the adult turkish population. *Clin Anat.* 2016; 29(2): 183–190, doi: [10.1002/ca.22634](https://doi.org/10.1002/ca.22634), indexed in Pubmed: [26403267](https://pubmed.ncbi.nlm.nih.gov/26403267/).
31. Yokota F, Otake Y, Takao M, et al. Automated muscle segmentation from CT images of the hip and thigh using a hierarchical multi-atlas method. *Int J Comput Assist Radiol Surg.* 2018; 13(7): 977–986, doi: [10.1007/s11548-018-1758-y](https://doi.org/10.1007/s11548-018-1758-y), indexed in Pubmed: [29626280](https://pubmed.ncbi.nlm.nih.gov/29626280/).